# Turbulent deposition and trapping of aerosols at a wall

John W. Brooke, K. Kontomaris, T. J. Hanratty, and John B. McLaughlin

Citation: Physics of Fluids A **4**, 825 (1992); doi: 10.1063/1.858299
View online: http://dx.doi.org/10.1063/1.858299
View Table of Contents: http://scitation.aip.org/content/aip/journal/pofa/4/4?ver=pdfcov
Published by the AIP Publishing

# Turbulent deposition and trapping of aerosols at a wall

John W. Brooke, K. Kontomaris, and T. J. Hanratty
*Department of Chemical Engineering, University of Illinois, Urbana, Illinois 61801*

John B. McLaughlin
*Department of Chemical Engineering, Clarkson University, Potsdam, New York, 13676*

(Received 8 February 1991; accepted 12 December 1991)

The trajectories of aerosols are computed in a high-resolution direct numerical simulation of turbulent flow in a vertical channel. The aerosol equation of motion includes only a Stokes drag force and the influence of the aerosols on the gas flow is assumed to be negligible. Since the flow is vertical, aerosols deposit as a consequence of the turbulent fluctuations and their own inertia. It is shown that the eddies which are responsible for aerosol deposition are the same eddies that control turbulence production. Typical aerosol trajectories are shown and related to eddy structure. A free-flight theory suggested by Friedlander and Johnstone [Ind. Eng. Chem. **49**, 1151 (1957)] is found to be based on reasonable assumptions about typical velocities of depositing aerosols as they pass through the viscous sublayer, but the theory is shown to be deficient in other respects. The distribution of normal velocities of the aerosols that deposit is compared to the distribution of fluid particle velocities in the viscous sublayer and some support is found for the notion that the probability distribution of Eulerian velocities may be useful in predicting deposition.

## I. INTRODUCTION

This paper presents new results pertaining to the motion of aerosols in the viscous wall region of a turbulent shear flow. The results were obtained from a high-resolution direct numerical simulation (DNS) of turbulent channel flow for $\mathrm{Re} = 9040$, where Re is the Reynolds number based on the hydraulic diameter of the channel.

The goals of the study were to identify the eddies that are primarily responsible for the deposition of aerosols, as well as their accumulation near walls, and to evaluate the free-flight theory of Friedlander and Johnstone.[1-3] The flow considered is a vertical flow of turbulent gas through a channel comprised of two infinite, parallel plates. The aerosols of interest typically have diameters of order 10 $\mu$m and densities that are 1000 times larger than the density of the gas; for such particles the sedimentation velocity is unimportant in comparison with the rms turbulent velocities for typical laboratory experiments with vertical flows.

In a previous paper, McLaughlin[4] reported the results of a study of aerosol motion in a low-resolution DNS of turbulent channel flow. He found that the aerosols that deposited on the walls possessed large normal components of velocity while they passed through the viscous sublayer; the typical values of these velocities were consistent with the values assumed in the Friedlander–Johnstone free-flight theory. However, no attempt was made to assess the other assumptions upon which Friedlander and Johnstone based their theory or to identify the eddies that are responsible for these large velocities. McLaughlin also reported that, when the initial aerosol seeding was uniform throughout the channel, an accumulation of aerosols near the walls developed after several hundred wall time units. The cause of this phenomenon was the inertia of the aerosols that enabled them to coast into the viscous sublayer where they have a large residence time. However, no attempt was made to estimate the residence time of the particles in the viscous sublayer or to obtain information about the mechanism that eventually enables them to escape. Kallio and Reeks,[5] as well as Sun and Lin,[6] also reported an accumulation of particles close to the wall.

The channel flow simulation in the present study involves a higher Reynolds number than the Reynolds number for which results were reported in Ref. 4. The pseudospectral methods used to solve the Navier–Stokes equation are the same as those described in Ref. 4, but larger periodicity lengths and smaller grid spacings were used in the present calculations. Lyons *et al.*[7] have given a detailed description of the effects of the grid spacing and the time step on the computed results. The periodicity lengths were sufficiently large that all two-point correlations became negligibly small when the horizontal separations were one-half the periodicity lengths; this was not true of the simulations used in Ref. 4. Finally, the grid spacings were sufficiently small to resolve all of the physically significant length scales.

In the present study, the particle equation of motion includes only the Stokes drag force. This introduces some error since, even for the smallest particles that deposit, the particle Reynolds number is of order unity as the particles pass through the viscous sublayer. In addition, wall effects are completely ignored in the calculations and a simple geometrical interception condition is used as the criterion for deposition; this evades the difficult question of how the particles penetrate to the wall. In spite of these gross oversimplifications, computed deposition rates are in order of magnitude agreement with the experimental measurements of deposition rates of olive oil droplets by Liu and Agarwal.[8]

 0899-8213/92/040825-10$04.00  

We have also performed calculations in which wall effects, nonlinear drag effects, and lift forces have been included in the particle equation of motion and have found that the issues on which we choose to focus in the present paper are not greatly affected by the presence or absence of these corrections. The results of calculations in which the additional forces are included will be presented in a future publication.

## II. PARTICLE EQUATION OF MOTION

The aerosols will be assumed to be small, rigid spherical particles that obey the following equation of motion derived by Maxey and Riley:[9]

$$\frac{d\mathbf{v}}{dt} = \frac{2(\rho-1)}{(2\rho+1)}g + \frac{2}{2\rho+1} \times\left(\frac{D\mathbf{u}}{Dt} + \frac{1}{2}\frac{d\mathbf{u}}{dt} + \frac{a^2}{20}\frac{d\nabla^2\mathbf{u}}{dt}\right) - \frac{9/(a^2\,\mathrm{Re})}{2\rho+1}\left(\mathbf{v}-\mathbf{u}-\frac{a^2}{6}\nabla^2\mathbf{u}\right) - \frac{9/(a\sqrt{\pi\,\mathrm{Re}})}{2\rho+1} \times\int_0^t \frac{(d/d\tau)[\mathbf{v}-\mathbf{u}-(a^2/6)\nabla^2\mathbf{u}]}{(t-\tau)^{1/2}}\,d\tau. \quad (1)$$

In the above equation, all physical quantities have been made nondimensional in terms of wall units based on the friction velocity, the kinematic viscosity, and the density of the fluid. Symbol $a$ denotes the particle radius, $\rho$ is the ratio of the particle density to the fluid density, and $g$ is the acceleration of gravity. Symbols $\mathbf{u}$ and $\mathbf{v}$ denote the fluid velocity and the particle velocity, respectively. The symbol $d/dt$ denotes a time derivative following the spheres, the $D/Dt$ denotes a time derivative using the undisturbed fluid velocity as the convective velocity. The fluid velocity is assumed to be unaffected by the presence of the particles and is supplied by the numerical simulation of channel flow. The terms on the right-hand side of Eq. (1) respresent the effects of gravity, virtual mass, Stokes drag, and history, respectively. The dimensionless particle relaxation time $\tau$ is defined as

$$\tau = [(2\rho+1)/9]a^2.$$

If it is assumed that $\rho \gg 1$ and that $\tau$ is of order unity, the radius of the particle in wall units must be small compared to unity. The terms on the right-hand side of Eq. (1) are of order $g$, $a^2$, 1, and $a$, so the equation of motion can be simplified to Eq. (1′)

$$\frac{d\mathbf{y}}{dt} = \frac{(\mathbf{u}-\mathbf{v})}{\tau}. \quad (1')$$

The acceleration due to gravity is assumed to have a negligible affect on the particle motion since the dimensionless gravitational constant $g$ is much smaller than unity for the aerosol particles considered. A detailed discussion of the derivation of Eq. (1′) can be found in Ref. 4. One difference with Ref. 4 is that the Saffman lift force is not considered in the present paper. The Saffman lift force contributes an additional term to the right-hand side of Eq. (1) of the form

$$\frac{d\mathbf{v}}{dt} = \left(\frac{0.0762a}{\tau}\right)\left|\frac{du_x}{dy}\right|^{1/2}(v_x-u_x)\hat{y}. \quad (2)$$

In Eq. (2), $d\mathbf{v}/dt$ is the dimensionless lift force divided by the particle mass acting on a rigid spherical particle in a unidirectional, time-independent shear flow that points in the $x$ direction and that is a function of $y$. The sign of the right-hand side of Eq. (2) is valid provided that $du_x/dy$ is positive. The quantity $\hat{y}$ denotes a unit vector in the $y$ direction. The Saffman lift force was found to have a significant effect on the rate of deposition, but the main focus in the present paper is on the fluid motions that bring the particles close to the wall and not on the rate of deposition.

It is interesting to note that the particle size and the density ratio do not independently appear in the equation of motion. In fact, the need to consider the particle size separately arises from the criterion for deposition—that the distance of the center of the aerosol from the wall is equal to $a$.

## III. NUMERICAL PROCEDURES

It is assumed that there is no feedback of the aerosols onto the gas flow since the particle number density and particle radii are both small. Thus, the fluid velocity field is obtained by a direct numerical solution of the Navier–Stokes equation:

$$\frac{\partial\mathbf{u}}{\partial t} = -\mathbf{u}\cdot\nabla\mathbf{u} - \nabla p + \nabla^2\mathbf{u} + g\mathbf{e}_1,$$

where $\mathbf{e}_1$ is a unit vector in the $x$-direction, $g$ is the acceleration of gravity, and $p$ is the pressure. The simulation is direct in the sense that no assumptions or models are used to simplify the fluid-dynamic equations. A pressure gradient which is sufficient to overcome the hydrostatic pressure and to accelerate the fluid vertically is the driving force for the flow. The fluid velocity is subject to rigid boundary conditions at the channel walls. In addition, the fluid is assumed to be incompressible:

$$\nabla\cdot\mathbf{u} = 0.$$

Periodic boundary conditions are imposed on the fluid velocity field in the streamwise ($x$) and spanwise ($z$) directions, respectively.

The pseudospectral methods used to solve the above equations are described in detail in Ref. 4. The present study differs only in the values of the periodicity lengths, the channel half-width, and the time step. The channel half-width was 150 wall units and the periodicity lengths were 1900 in the downstream direction and 950 in the spanwise direction, compared to 125, 630, and 630 in Ref. 4. The time step used in the present study was 0.25 wall units, while the time step used in Ref. 4 was 0.2. The numbers of grid points in the $x$, $y$, and $z$ directions were 128, 65, and 128, respectively. The corresponding grid spacings in the $x$ and $z$ directions were 14.8 and 7.4. The grid spacing in the $y$ direction was 0.18 near the walls and increased to 7.4 near the center of the channel. The nonlinear terms were evaluated on this grid. However, the 2/3 rule suggested by Orszag[10] was used to reduce aliasing in the $x$ and $z$ directions. As a result, in the $x$ and $z$ directions, the smallest length that could be resolved was 50% larger than the grid spacings in $x$ and $z$. Lyons *et al.*[7] have found that this spatial resolution is sufficient to describe the significant length scales in the channel flow.

In solving the Navier–Stokes equation by pseudospec-

tral methods, the fluid velocity field is expanded in a three-dimensional Fourier–Chebyshev series in which the variations in the $x$ and $z$ directions are represented by Fourier series and the variations in the $y$ direction are represented by a Chebyshev series. In Ref. 4, the undisturbed fluid velocity at the center of the aerosol was obtained by computing the Fourier–Chebyshev sum. However, the finer grid resolution used in the present study permitted the use of a hybrid interpolation scheme in which the exact Chebyshev sum is performed for the $y$ coordinate of the particle at a set of points surrounding the particle and having the same $x$ and $z$ coordinates as the grid points. Lagrange interpolation of order 6 is then performed in the $x$ and $z$ directions in order to estimate the undisturbed fluid velocity at the center of the particle. Kontomaris *et al.*[11] have evaluated the accuracy of this procedure in tracking point particles and have shown that it is highly accurate for the same flow conditions used in the simulations to be reported. The operation count for the above scheme is smaller by roughly the factor $(6/N_x)(6/N_z)$ than the operation count for a fully spectral evaluation of the fluid velocity at the particle location. A fully spectral evaluation of the fluid velocity would involve summing the Fourier–Chebyshev series of the undisturbed fluid velocity at the point occupied by the center of the particle.

## IV. PARAMETER CHOICES

In the calculations to be reported, the density ratio $\rho$ was chosen to be 713, which corresponds to olive oil in air. The value of the particle relaxation time $\tau$ was chosen to be 0, 3, 5, 7, and 10. The corresponding values of the particle radius $a$ are 0, 0.138, 0.178, 0.210, and 0.238. In dimensional terms, the particle radius values are $av/u^*$. For air flowing in a 1 in. pipe, the dimensional values of the particle radius would be approximately (in micrometers) 0, 13.8, 17.8, 21.0, and 23.8. The dimensionless gravitational constant $g$ for this flow is approximately 0.0436, which is less than 5% of the typical acceleration seen by particles which deposit.

The number of particles used in the computer experiment was 16 129. The particles were uniformly distributed over a plane at 40 wall units from one of the two channel walls, which will be referred to as the bottom channel wall for convenience. The initial velocity of each particle was set equal to the local undisturbed fluid velocity evaluated at the center of the particle. The run was performed for a total of 200 time wall units.

## V. RESULTS

In Fig. 1, the probability density of finding a particle in a bin of width unity in the $y$ direction is plotted as a function of distance measured from the bottom channel wall for three times. The three curves in each graph correspond to fluid particles and particles with $\tau = 5$ and 10. It can be seen that the particles diffuse over a significant portion of the channel over the time of the simulation. The initial diffusion from $y = 40$ to larger values of $y$ is very nearly Gaussian and the diffusion constant of aerosols is somewhat larger than for fluid particles. The value of the diffusion constant for fluid particles in wall units is 21.9 and for $\tau = 10$ it is 28.0. The

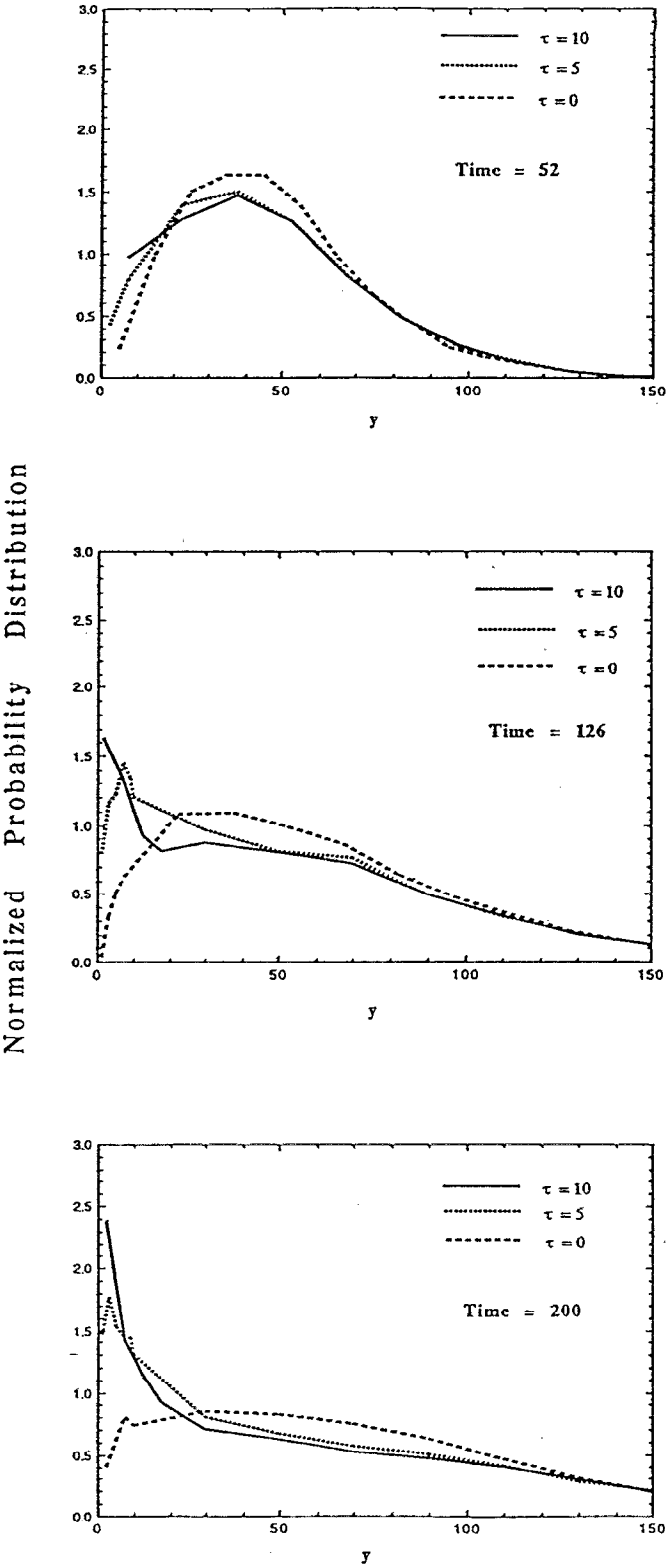


FIG. 1. Normalized probability distributions at different times.

value of 21.9 is approximately twice the long-time Lagrangian diffusivity in the normal direction, 9.88, of fluid particles released at the center (Kontomaris[12]).

It is interesting to note that the aerosols tend to accumulate near the wall. McLaughlin[4] noted a similar phenomenon

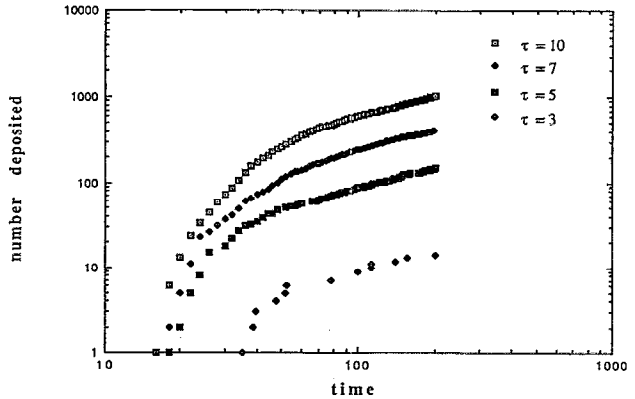


FIG. 2. The influence of $\tau$ on the number of particles deposited.

with aerosols having $\tau = 2$ in his low-resolution study. For $\tau = 10$, the point of maximum concentration is at the wall (the particles that have deposited are not included in the probability distribution so this statement must be understood in a limiting sense), while the maximum is located at a finite distance from the wall for the fluid particles. This accumulation at the wall can be interpreted as a turbophoresis phenomenon whereby the flux toward the wall due to gradients in fluid turbulence is larger than the flux away from the wall due to diffusion.

In Fig. 2, the number of particles that have deposited is plotted as a function of time measured from the beginning of the run. It can be seen that the rate of deposition approaches a constant value at large times in all cases. This result is surprising, considering the accumulation of particles in the viscous sublayer. In fact, the deposition rate actually decreases slightly with time, which suggests that the particles that accumulate near the wall do not deposit on the wall. Further evidence to support this notion will be supplied in what follows.

Liu and Agarwal[8] found that the deposition rate data vary quadratically with relaxation time in experiments in which olive oil droplets were uniformly distributed in a vertical pipe flow. It is not possible to make a detailed comparison with their results because of the differences in the two experiments. In Fig. 3 the slopes of the curves in Fig. 2 over the last 100 time units are plotted versus the square of the particle relaxation time. It can be seen that the computed results are roughly consistent with the laboratory findings if one assumes that the concentration of particles in the region from which the deposition particles originate is the same for particles having different relaxation times. The actual deposition velocity is about four times smaller than the deposition velocity reported by Liu and Agarwal for $\tau = 10$ if one bases the calculation on the particle concentration at around 40 units from the bottom wall. There are several possible reasons for the discrepancy. There are significant variations in the particle concentration in our calculations. It is not clear which concentration to use in computing a deposition velocity and our choice is, admittedly, only a guess. We have also neglected forces such as Saffman's lift force that may affect the deposition rate. It will be seen later that large numbers of particles almost reach the wall; even a modest force acting on these particles could cause them to deposit. The strong dependence of deposition rate on particle size implies that small variations in droplet size could cause significant variations in deposition rate.

In Fig. 4, the trajectories of four particles having different relaxation times but starting from the same initial position are shown. The three largest particles travel along similar trajectories and all strike the bottom wall, but the smallest particle is pulled sideways near the wall and never deposits. The trajectories of the aerosols are consistent with the instantaneous flow field at the beginning of the run, which is shown in Fig. 5.

Friedlander and Johnstone suggested that aerosols execute a free flight to the wall over the stopping distance of a particle in a stagnant fluid. The velocity of the aerosol at the beginning of its free flight was taken to be 0.91, which is the

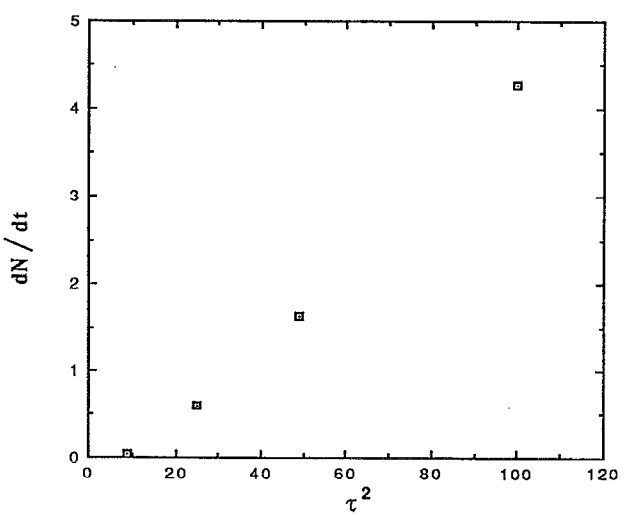


FIG. 3. Rate of deposition over the time interval of 100–200.

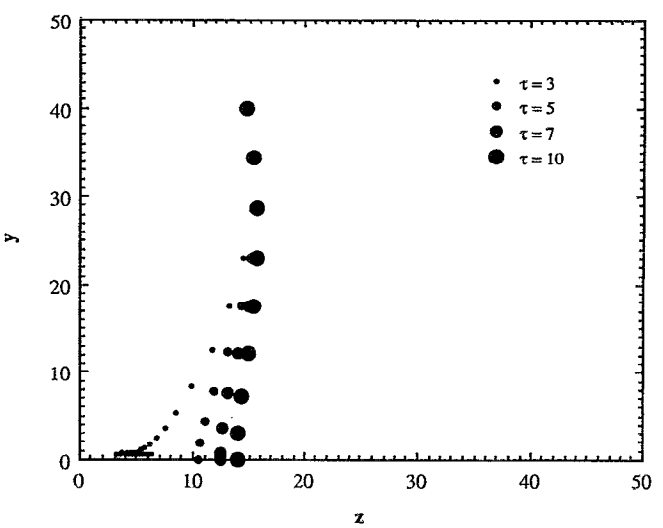


FIG. 4. Trajectories of particles of different sizes—starting from the same point.

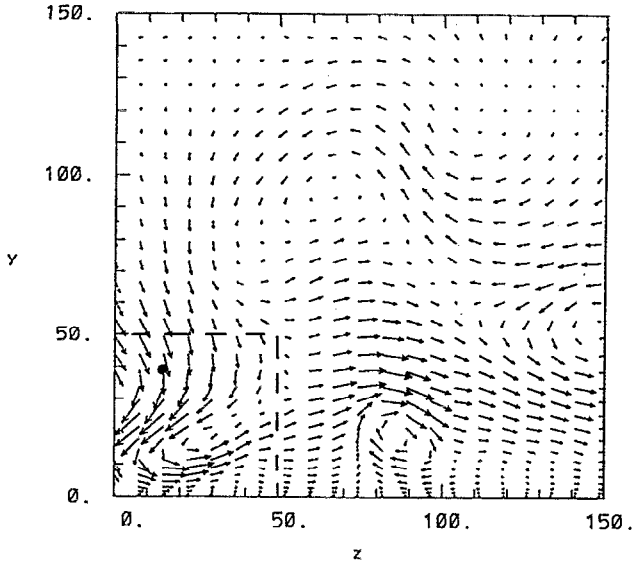


FIG. 5. Instantaneous velocity field at the initial $x$ location of the particles.

value of the turbulent intensity in the outer flow. In Fig. 6, the conditionally averaged normal component of the particle velocity versus distance from the wall for $\tau = 5$ and 10 are plotted as the solid and dashed curves. The condition on which the average is based is that the particle should deposit on the wall. In the same graph, the velocities required for the particles to reach the wall by free flight are indicated by the squares and diamonds. The intersection of the two plots for each value of $\tau$ can be interpreted as the maximum distance from the wall at which the particle, on average, can reach the wall in free flight. The velocities of individual particles vary widely. The significance of the point of intersection is that a particle moving with the average velocity has sufficient momentum to reach the wall even if the fluid is stagnant. The point of intersection occurs for an average velocity in the range 0.5–0.8. This is much larger than the local intensity and close to the value of 0.9 suggested by Friedlander and

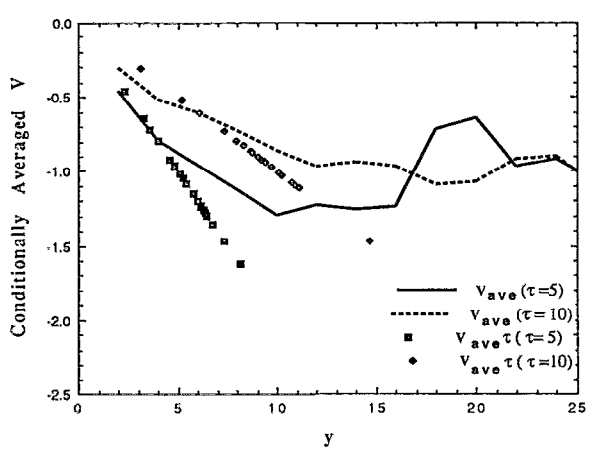


FIG. 6. Conditionally averaged velocity component of depositing particles.

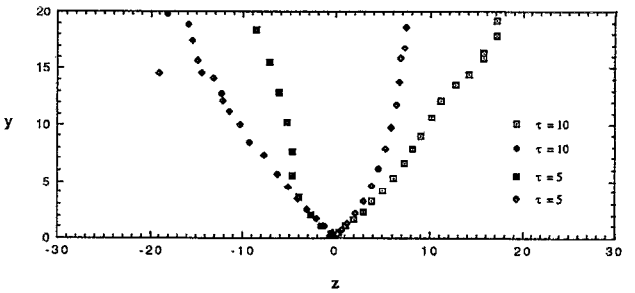


FIG. 7. Conditionally averaged trajectories of depositing particles in the $y$-$z$ plane.

Johnstone. However, it will be shown that, in other respects, the Friedlander–Johnstone theory is deficient. For example, in formulating their model, they assume that the aerosols diffuse to the stopping distance and then execute a free flight to the wall. At the stopping distance, they assume that all particles move on a free flight to the wall. The results in this paper do not support this notion; only a small fraction of the particles at the stopping distance travel to the wall because the particle velocity averaged over all particles at the stopping distance is much smaller than the conditionally averaged particle velocity. Some new results indicate that turbophoresis is responsible for bringing particles to the stopping distance.

Figure 7 shows a projection onto the $y$-$z$ plane of conditionally averaged trajectories. The trajectories have been translated so that they have a common point of impact before performing the average. In addition, particles that strike the wall with positive $z$ components of velocity have been averaged with other particles moving in the positive $z$ direction and, similarly, for negative velocities. It is interesting to note that the particles strike the wall approximately at a 45° angle regardless of the value of $\tau$. Similar behavior can be seen in the individual trajectories shown in Fig. 4, suggesting that these particles are flung to the wall by eddies which impart strong spanwise motion to the particle trajectories before they deposit. A $y$-$z$ projection of the average eddies responsible for the deposition of $\tau = 10$ particles is shown in Fig. 8. The condition used in obtaining the average is that a depositing particle is present at $y = 20$ and that it has a positive $z$ velocity just before deposition. At $y = 20$ the conditionally averaged particle velocity toward the wall reaches a maximum. The resulting conditional eddy is arbitrarily centered about $z = 475$. The eddies appear to be the same eddies that Lyons *et al.*[7] have identified as controlling turbulence production in the viscous wall region.

Figure 9 shows four typical flow patterns seen by $\tau = 10$ depositing particles when they are at $y = 20$. The arrows indicate turbulence producing quasistreamwise vortices and the dots are the particle locations at $y = 20$. The circled regions on the sides of the eddies are areas of high Reynolds stresses, $-uv > 3.5$, which indicates high turbulence production. The centers of the structures indicated by the arrows in Fig. 9 are regions of high streamwise vorticity. The center of these vortices typically have values of streamwise

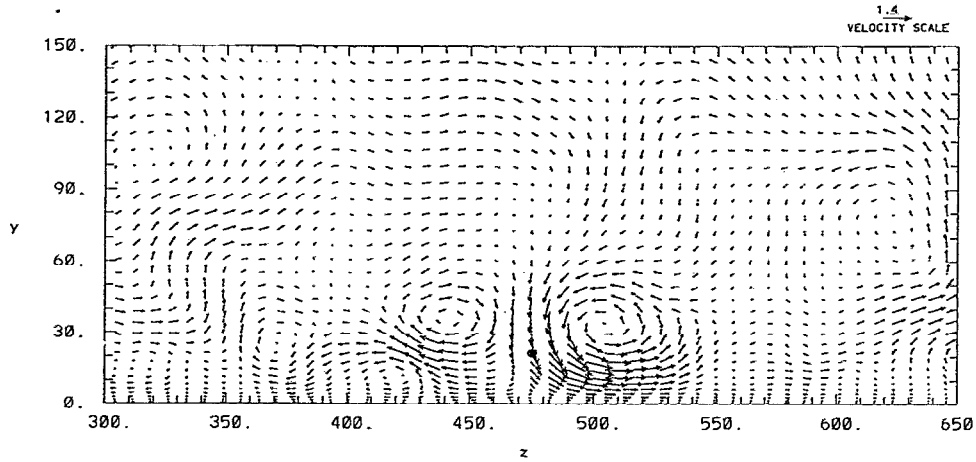


FIG. 8. Average field seen by depositing particles when they are at $y = 20$ with a positive $z$ component of velocity at deposition.

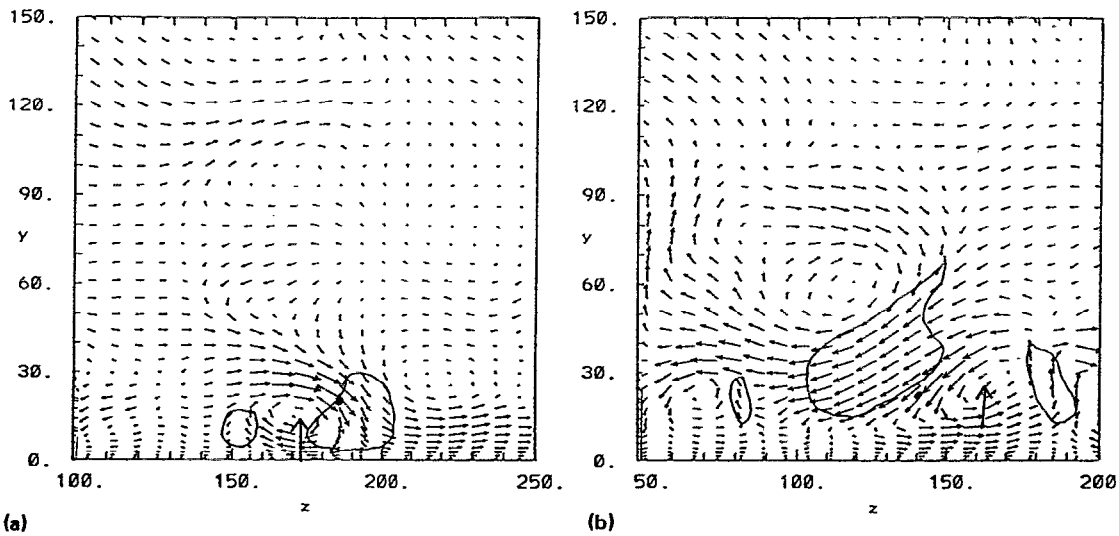


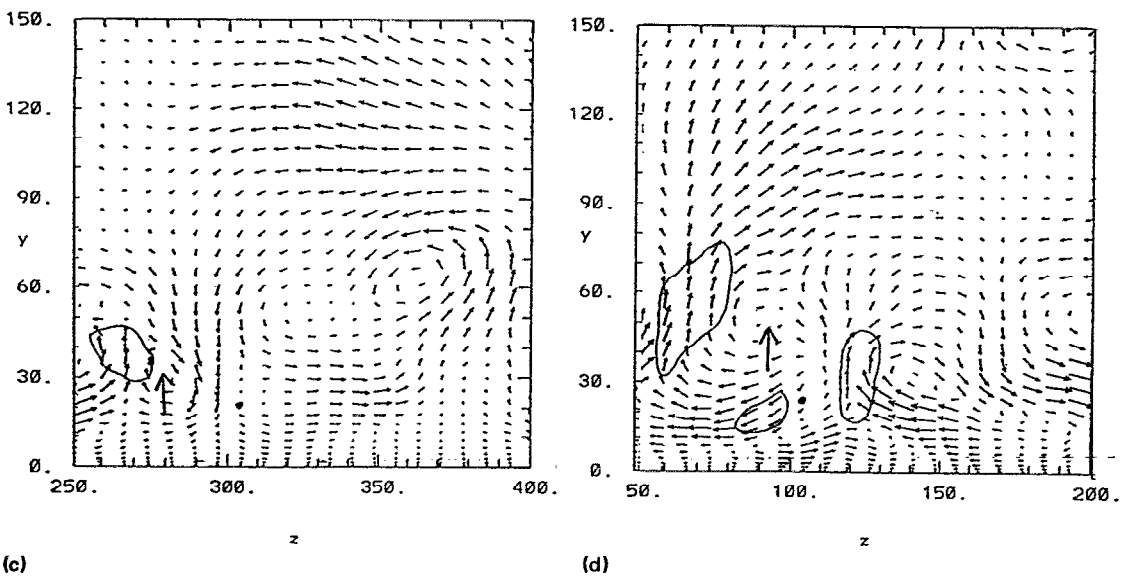


FIG. 9. Instantaneous flow fields seen by depositing particles when they are at $y = 20$ ( $-uv > 3.5$).

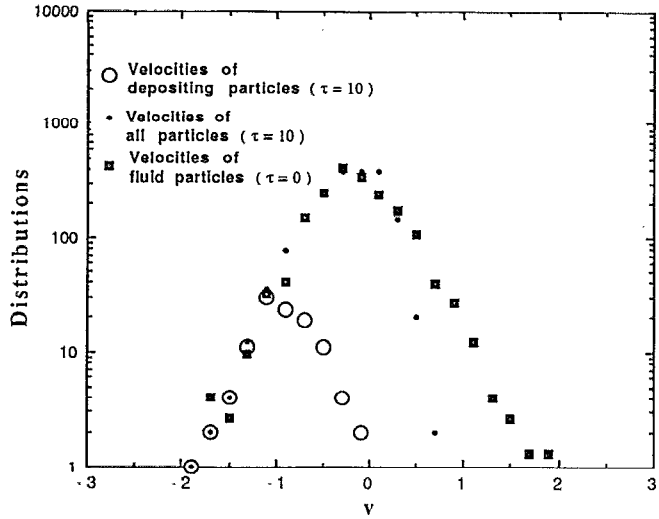


FIG. 10. Distribution functions at $y = 10$ for velocities of the fluid, particles, and for the subset of particles that deposit before the run is terminated at $t = 200$.

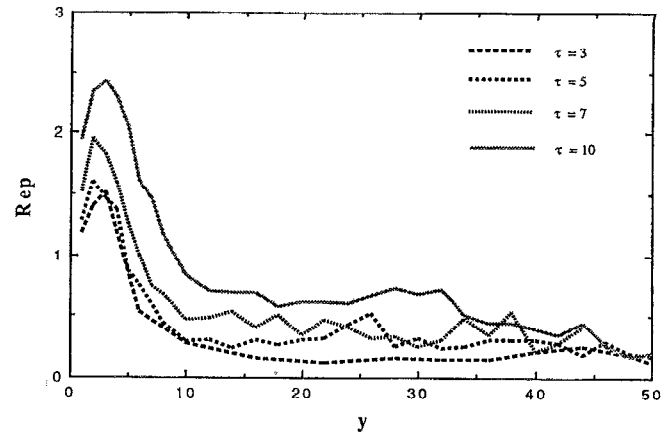


FIG. 12. Average particle Reynolds numbers of depositing particles.

vorticity $\omega_x = 0.3$ at $y = 20$. This is approximately twice the root-mean-square value of $\omega_x$ at this distance from the wall. The most common flow feature responsible for deposition was observed to be streamwise vortices centered between $y = 15$ and 30 with average diameter $\Delta z = 25$ and whose streamwise dimension varied from $\Delta x = 200$ to 800. Direct observation of rotational motions by several investigators (Moser and Moin,[13] Robinson *et al.*,[14] Guezennec *et al.*,[15] and Brooke[16]) have shown that single streamwise-oriented vortices are statistically more probable than pairs of equal strength. The streamwise vortices associated with deposition were observed to be single vortices in more than 75% of the observations. Occasionally, a counter-rotating vortex such as in Fig. 9(b) at $y = 60$ and $z = 110$ was observed.

In Fig. 10, the number of particles and the number of depositing particles are shown for $\tau = 10$ at $y = 10$ as a function of the velocity toward the wall. The probability distribution for the fluid particles released at the same initial location as the $\tau = 10$ particles is also included in the same plot. The tail of the fluid particle distribution coincides with the distribution for depositing particles at large negative velocities. The peak of the distribution of depositing particles occurs at approximately $v = -1$. It is to be noted that for $\tau = 5$ similar results to those shown in Fig. 10 are obtained at $y = 5$ with a maximum again at $v \approx -1$. The fluid particle distribution is similar in nature to an Eulerian velocity distribution. This suggests that it might be feasible to use results such as these to estimate aerosol deposition rates from Eulerian probability distributions of fluid velocities. This might be accomplished by integrating the Eulerian velocity probability distribution from $v \approx -1$ to $v \approx -\infty$ at the free-flight distance to obtain a flux of particles moving toward the wall. If all depositing particles start their free flight from roughly the same distance, this flux could then be used to approximate the flux of depositing particles at the wall.

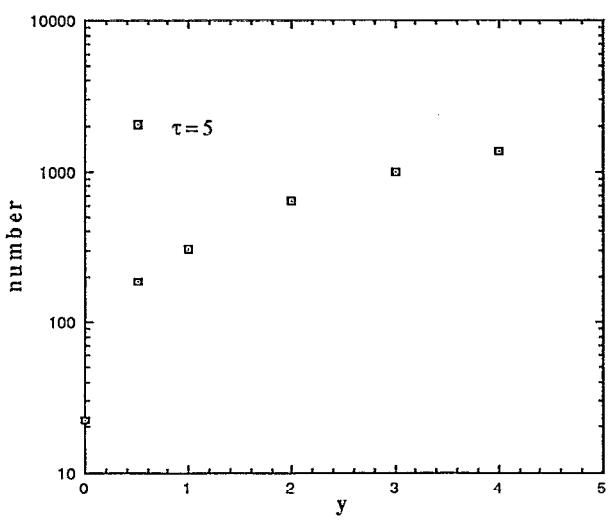


FIG. 11. Number of particles reaching a given distance from the wall over the time interval of 150–200.

The criterion for deposition used in this paper is simplistic so it is important to determine how sensitive the results are to its choice. In Fig. 11, the number of particles with $\tau = 5$ that pass a given $y$ in a fixed period of time (150 to 200) is given. It is noted that this number increases dramatically with distance from the wall. It is of interest to note that, for the particles that deposit, the particle Reynolds number based on the particle diameter and the translation velocity relative to the undisturbed fluid is not small compared to unity in the viscous sublayer. This is shown in Fig. 12 where the conditionally averaged particle Reynolds number is plotted versus distance from the wall for different values of $\tau$. Thus, nonlinear drag corrections will play a significant role in the trajectories of the particles. Such corrections, as well as other forces, have been considered in a different study. It is found that, although the rate of deposition is strongly affected, the conditionally averaged profiles are not greatly modified.

Figure 13 shows end views of three typical trajectories of particles with $\tau = 5$ that deposit a long time after their re-

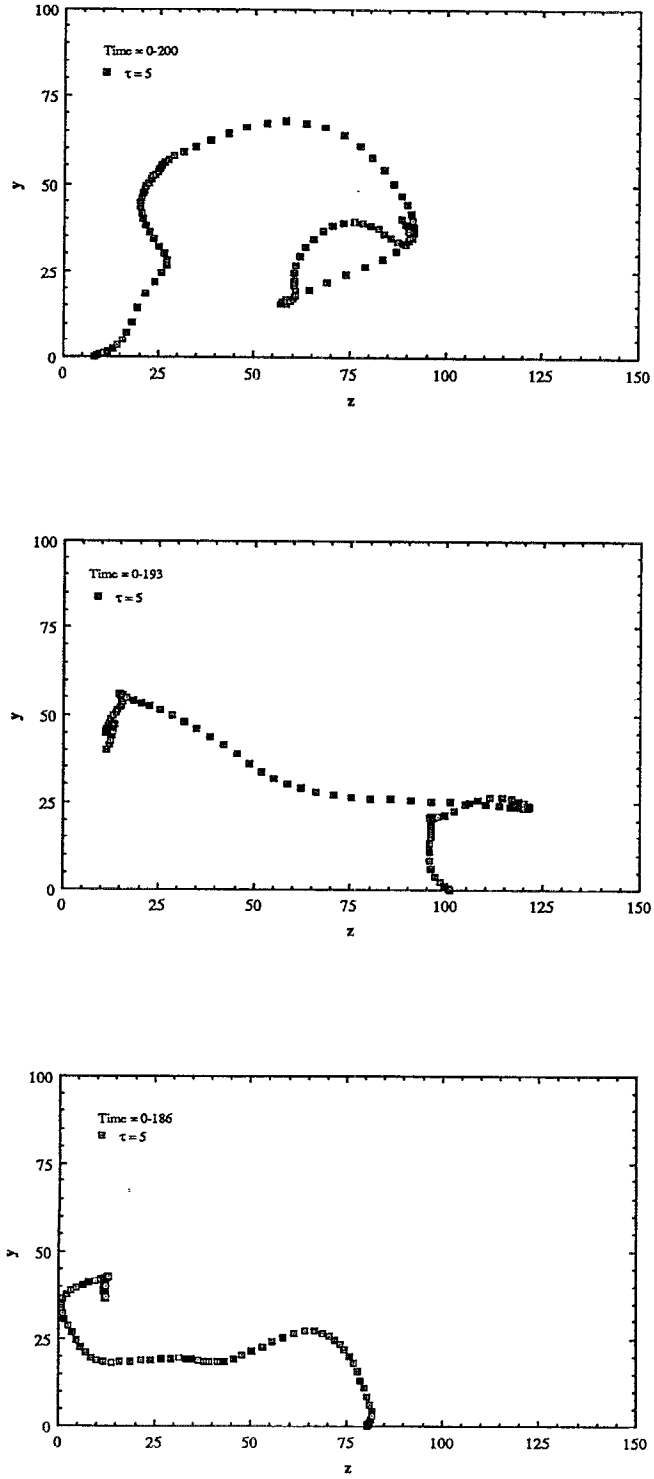


FIG. 13. Examples of trajectories of depositing particles in the $y$-$z$ plane.

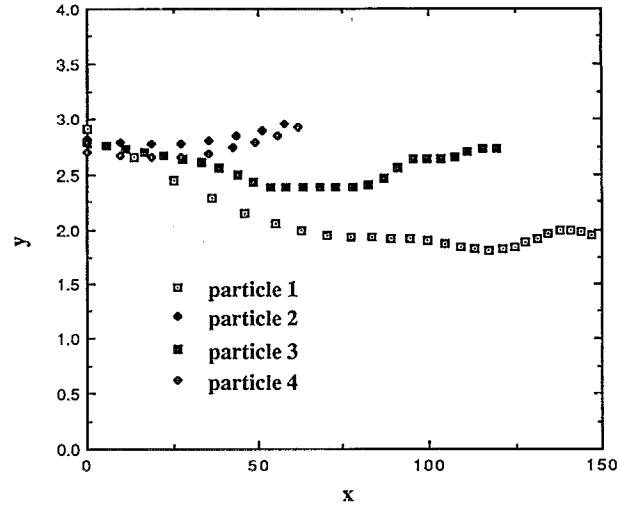


FIG. 14. Typical trajectories of particles that crossed $y = 3$ but did not deposit.

lease. Typically a particle wanders sideways until it is trapped in a strongly correlated motion which brings it directly to the wall. This correlated motion typically begins at a distance 20 to 30 wall units from the wall. Very close to the wall, the particle is pulled sideways because of spanwise motions which, in the viscous sublayer, are much stronger than the motions toward the wall. Figure 14 shows typical trajectories of particles trapped in the region $y<3$. Figure 15 shows the streamwise and spanwise coordinates of $\tau = 3$ and $\tau = 10$ particles for the region $0<y<5$ at time $= 200$. The instantaneous streamwise–spanwise velocity vectors at time $= 200$ and at $y = 3$ are also shown. The flow is from left to right and the mean velocity has been subtracted from the streamwise velocity vector. It appears that there is a weak tendency for particles to accumulate in low-speed streaks, especially for the $\tau = 3$ particles. The mechanism for particle transport has been described by Kline *et al.*[17] and by Rashidi and Banerjee.[18] This mechanism proposes that particles accumulate in low-speed streaks and are lifted up by vortex loops as part of an ejection process. Rashidi and Banerjee report that particles with $\tau = 5$–10 tend to accumulate in low-speed streaks. Results from this investigation have not indicated conclusively whether $\tau = 5$–10 aerosol particles accumulate in low-speed streaks. Rashidi and Banerjee also report that particles that fall beneath the viscous sublayer whose dimensionless radius $a$ is less than 0.5 do not interact with the bursting process and are rarely lifted up by the wall ejections. Similar conclusions were reached from this investigation.

## VI. CONCLUSIONS

It has been shown that the free-flight theory of Friedlander and Johnstone is based on correct assumptions about the free-flight velocity but that the theory is defective in other ways. At any point in the viscous sublayer, only a small fraction of the particles are undergoing a free flight to the wall. It has been shown that the eddies that are responsible for deposition are virtually the same as the eddies that control the production of turbulence in the viscous sublayer.

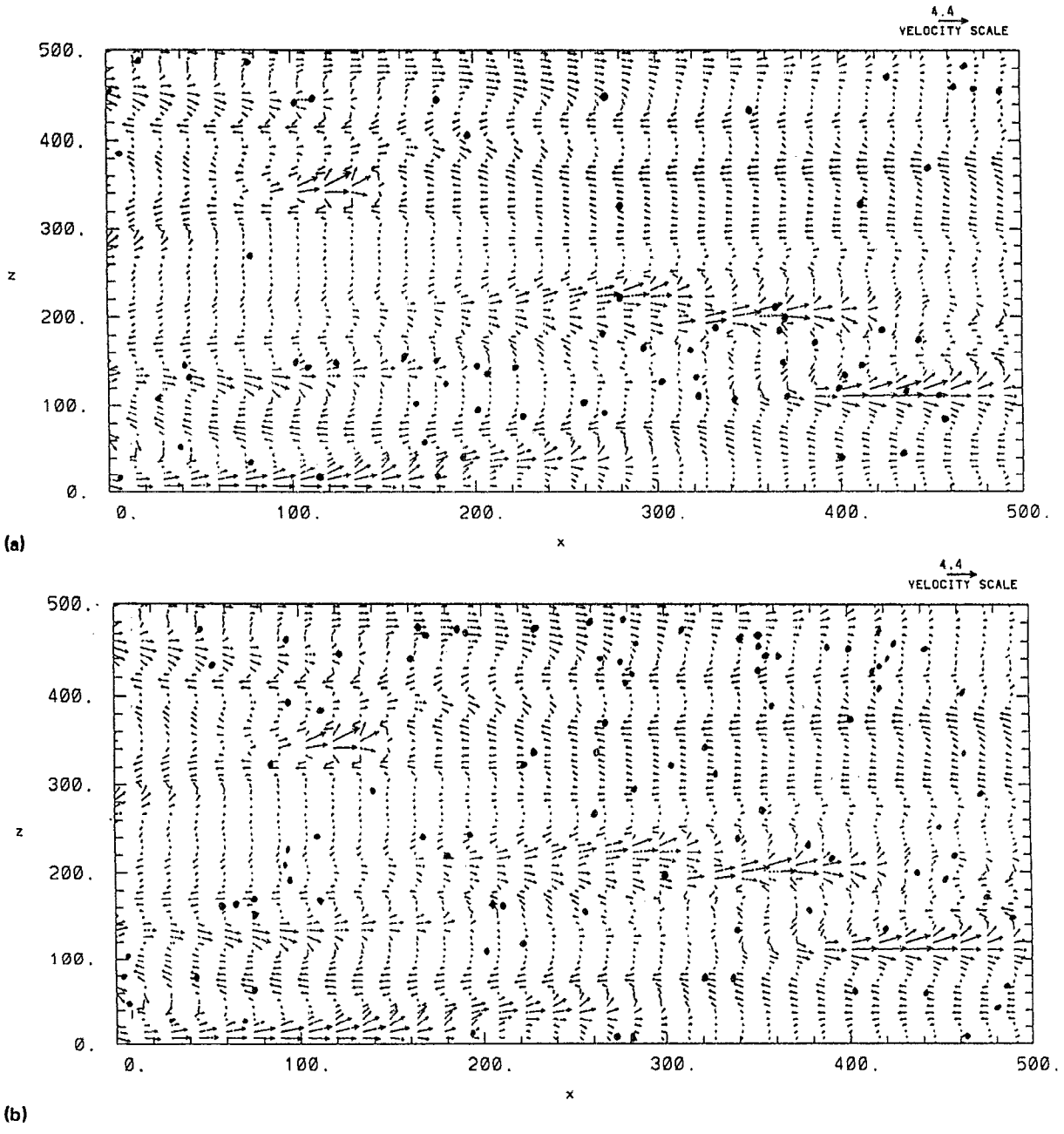


FIG. 15. Streamwise–spanwise location at $t = 200$ and $0 < y < 5$ for (a) $\tau = 3$ and (b) $\tau = 10$ particles and the streamwise–spanwise instantaneous velocity vectors at $t = 200$ and $y = 3$.

Conditionally averaged particle trajectories indicate that, on average, the particles that strike the wall are moving at a 45° angle in the $y$-$z$ plane. It seems promising that the probability distribution of Eulerian fluid velocities might be used to estimate the deposition rates that will be observed for a given value of the particle relaxation time.

## ACKNOWLEDGMENTS

We acknowledge the support and facilities of the National Center for Supercomputing Applications at the University of Illinois, Urbana and the Cornell National Supercomputer Facility.

This work was supported by the U.S. Department of Energy (Contract No. DEF 602-86ER13556) and by the Transport Phenomena Program of the National Science Foundation (Grant No. CTS 89-19843). J. B. M. acknowledges support from the U.S. Department of Energy under Contract No. DE-FG02-88ER13919.

[1] S. K. Friedlander and H. F. Johnstone, "Deposition of suspended particles from turbulent gas streams," Ind. Eng. Chem. **49**, 1151 (1957).
[2] G. A. Sehmel, "Particle deposition from turbulent air flow," J. Geophys. Res. **5**, 1766 (1970).

[3]G. A. Sehmel, "Particle diffusivities and deposition velocities over a horizontal smooth surface," J. Colloid Interface Sci. **37**, 891 (1971).
[4]J. B. McLaughlin, "Aerosol particle deposition in numerically simulated channel flow," Phys. Fluids A **1**, 1211 (1989).
[5]G. A. Kallio and M. W. Reeks, "A numerical simulation of particle deposition in turbulent boundary layers," Int. J. Multiphase Flow **15**, 433 (1989).
[6]Y. F. Sun and S. P. Lin, "Aerosol concentration in a turbulent flow," J. Colloid Interface Sci. **113**, 315 (1986).
[7]S. L. Lyons, T. J. Hanratty, and J. B. McLaughlin, "Large-scale computer simulation of fully developed turbulent channel flow with heat transfer," Int. J. Numer. Methods Fluids **13**, 999 (1991).
[8]B. Y. H. Liu and J. K. Agarwal, "Experimental observation of aerosol deposition in turbulent flow," J. Aerosol Sci. **5**, 145 (1974).
[9]M. R. Maxey and J. J. Riley, "Equation of motion for a small rigid sphere in a nonuniform flow," Phys. Fluids **26**, 883 (1983).
[10]S. A. Orszag, "On the elimination of aliasing in finite-difference schemes by filtering high-wavenumber components," J. Atmos. Sci. **28**, 1074 (1971).
[11]K. Kontomaris, T. J. Hanratty, and J. B. McLaughlin, "An algorithm for tracking fluid particles in a spectral simulation of turbulent channel flow," submitted to J. Comput. Phys. (1990).
[12]K. Kontomaris, "Point source dispersion in a direct numerical simulation of turbulent channel flow," Ph.D. thesis, University of Illinois at Urbana/Champaign, 1991.
[13]R. D. Moser and P. Moin, "Direct numerical simulation of curved turbulent channel flow," NASA Tech. Memo. 85974 (1984).
[14]S. K. Robinson, S. J. Kline, and P. R. Spalart, "A review of quasi-coherent structures in a numerically simulated turbulent boundary layer," NASA Tech. Memo. 102191 (1989).
[15]Y. G. Guezennec, U. Piomelli, and J. Kim, "On the shape and dynamics of wall structures in turbulent channel flow," Phys. Fluids A **1**, 764 (1989).
[16]J. W. Brooke, "A study of coherent eddy structure in turbulent channel flow," M.S. thesis, University of Illinois at Urbana/Champaign, 1991.
[17]S. J. Kline, W. C. Reynolds, F. A. Schraub, and P. W. Runstadler, "The structure of turbulent boundary layers," J. Fluid Mech. **30**, 741 (1967).
[18]M. Rashidi and S. Banerjee, "The effect of boundary conditions and shear rate on streak formation and breakdown in turbulent channel flow," Phys. Fluids A **2**, 1827 (1990).